Journal of Astronomical Telescopes, Instruments, and Systems

AstronomicalTelescopes.SPIEDigitalLibrary.org

Design, implementation, and performance of the Astro-H soft x-ray spectrometer aperture assembly and blocking filters

Caroline A. Kilbourne
Joseph S. Adams
Petar Arsenovic
Travis Ayers
Meng P. Chiao
Michael J. DiPirro
Megan E. Eckart
Ryuichi Fujimoto
John D. Kazeva
Kari L. Kripps
Bruce M. Lairson
Maurice A. Leutenegger
Heidi C. Lopez
Dan McCammon
Daniel S. McGuinness
Kazuhisa Mitsuda
Samuel J. Moseley
F. Scott Porter
Andrea N. Schweiss
Yoh Takei
Rosemary Schmidt Thorpe
Tomomi Watanabe
Noriko Y. Yamasaki
Seiji Yoshida

Caroline A. Kilbourne, Joseph S. Adams, Petar Arsenovic, Travis Ayers, Meng P. Chiao, Michael J. DiPirro, Megan E. Eckart, Ryuichi Fujimoto, John D. Kazeva, Kari L. Kripps, Bruce M. Lairson, Maurice A. Leutenegger, Heidi C. Lopez, Dan McCammon, Daniel S. McGuinness, Kazuhisa Mitsuda, Samuel J. Moseley, F. Scott Porter, Andrea N. Schweiss, Yoh Takei, Rosemary Schmidt Thorpe, Tomomi Watanabe, Noriko Y. Yamasaki, Seiji Yoshida, "Design, implementation, and performance of the Astro-H soft x-ray spectrometer aperture assembly and blocking filters," *J. Astron. Telesc. Instrum. Syst.* **4**(1), 011215 (2018), doi: 10.1117/1.JATIS.4.1.011215.

SPIE.

Design, implementation, and performance of the Astro-H soft x-ray spectrometer aperture assembly and blocking filters

Caroline A. Kilbourne,[a,*] Joseph S. Adams,[a,b] Petar Arsenovic,[a] Travis Ayers,[c] Meng P. Chiao,[a,b] Michael J. DiPirro,[a] Megan E. Eckart,[a] Ryuichi Fujimoto,[d] John D. Kazeva,[a,e] Kari L. Kripps,[f] Bruce M. Lairson,[c] Maurice A. Leutenegger,[a,b] Heidi C. Lopez,[c] Dan McCammon,[f] Daniel S. McGuinness,[a] Kazuhisa Mitsuda,[g] Samuel J. Moseley,[a,h] F. Scott Porter,[a] Andrea N. Schweiss,[a] Yoh Takei,[g] Rosemary Schmidt Thorpe,[a,i] Tomomi Watanabe,[a,j] Noriko Y. Yamasaki,[g] and Seiji Yoshida[k]

[a]NASA Goddard Space Flight Center, Greenbelt, Maryland, United States
[b]University of Maryland, Center for Space Sciences and Technology, Baltimore County, Baltimore, Maryland, United States
[c]Luxel Corporation, Friday Harbor, Washington, United States
[d]Kanazawa University, Faculty of Mathematics and Physics, Kanazawa, Ishikawa, Japan
[e]SGT, Inc., Greenbelt, Maryland, United States
[f]University of Wisconsin, Department of Physics, Madison, Wisconsin, United States
[g]ISAS/JAXA, Sagamihara, Kanagawa, Japan
[h]ADNET Systems, Inc., Bethesda, Maryland, United States
[i]Bastion Technologies Inc., Houston, Texas, United States
[j]University of Maryland, Department of Astronomy, College Park, Maryland, United States
[k]Sumitomo Heavy Industries, Ltd., Niihama, Ehime, Japan

Abstract. The calorimeter array of the JAXA Astro-H (renamed Hitomi) soft x-ray spectrometer (SXS) was designed to provide unprecedented spectral resolution of spatially extended cosmic x-ray sources and of all cosmic x-ray sources in the Fe-K band around 6 keV. The properties that made the SXS array a powerful x-ray spectrometer also made it sensitive to photons from the entire electromagnetic band as well as particles. If characterized as a bolometer, it would have had a noise equivalent power of $<4 \times 10^{-18}$ W/$(\mathrm{Hz})^{0.5}$. Thus, it was imperative to shield the detector from thermal radiation from the instrument and optical and UV photons from the sky. In addition, it was necessary to shield the coldest stages of the instrument from the thermal radiation emanating from the warmer stages. These needs were addressed by a series of five thin-film radiation-blocking filters, anchored to the nested temperature stages, that blocked long-wavelength radiation while minimizing x-ray attenuation. The aperture assembly was a system of barriers, baffles, filter carriers, and filter mounts that supported the filters and inhibited their potential contamination. The three outer filters also had been equipped with thermometers and heaters for decontamination. We present the requirements, design, implementation, and performance of the SXS aperture assembly and blocking filters. [DOI: 10.1117/1.JATIS.4.1.011215]

Keywords: x-ray calorimeter; microcalorimeter; radiation-blocking filters; aperture cylinder; Astro-H; Hitomi.

Paper 17057SSP received Aug. 15, 2017; accepted for publication Jan. 22, 2018; published online Feb. 26, 2018.

1 Introduction

The detectors[1] of the Hitomi soft x-ray spectrometer (SXS) instrument[2] were anchored to a 50-mK heat sink provided by a multistage and partially redundant cooling system.[3,4] The low-temperature stages resided within a dewar with a main-shell temperature of about 260 K in orbit. Thus, the instrument aperture was a series of openings in stages at temperatures spanning from 50 mK to 260 K. The main objective of the aperture assembly (ApA) was to block visible, infrared, and ultraviolet light via thin-film blocking filters (BF), while allowing x-rays to pass through with minimal absorption. The ApA accommodated radiation BF and associated mechanical, thermal, and electrical hardware. The ApA was designed to prevent water vapor and other contaminants from collecting on the BFs or penetrating into the dewar, and the accommodation for filter heaters provided decontamination capability.

The SXS design derived considerable heritage from the design of the calorimeter-based x-ray spectrometer (XRS) of Suzaku and Astro-E, and the starting points for the ApA and BF design for SXS were the similar subsystems of XRS.[5–7] The XRS design consisted of five aluminum-coated, polyimide, thin-film filters, with the two warmest filters closing out a cylindrical contamination barrier consisting of a gamma-alumina fiber-epoxy composite tube with a Ti foil liner. The two warmest filters were equipped with decontamination heaters. That basic system outline was preserved for SXS, but because of major differences in the cooling system, the temperatures and spacing of the intermediate filters were required to change. In addition, progress in blocking-filter technology, specifically the use of silicon supporting meshes, was applied to the new mission to increase the strength of the larger filters, minimize the impact of localized damage to any of the thin films, and enhance the effectiveness of heating elements placed on the filter frames.

*Address all correspondence to: Caroline A. Kilbourne, E-mail: caroline.a.kilbourne@nasa.gov

2 High-Level System Design

2.1 *Components*

There were a total of nine separate subassemblies that composed the combined ApA and BF subsystem. The name of each was derived from the dewar interface to which it attached mechanically and thermally. These interfaces are listed and defined in Table 1.

The ApA was integrated into the dewar one subassembly at a time and never constituted a complete assembly by itself outside of the dewar. Starting from the inside and progressing outward, these subassemblies and their interfaces were as follows:

1. Calorimeter thermal sink lid filter (CTSL-F): The calorimeter thermal sink (CTS) was the detector enclosure regulated at 50 mK. The CTS was suspended within the structure of the DA (detector assembly) that ran nominally at 1.3 K. Design details of the DA are found in Ref. 8. The CTSL-F closed out the detector enclosure. The CTS filter was permanently integrated into the CTS lid; thus, it was the first ApA component integrated into the SXS dewar.
2. Detector assembly lid (DAL): The DAL was the top close-out to the DA, and it supported the DAL-FC (#3) via an o-ring.
3. Detector assembly lid filter/carrier (DAL-FC): The DAL-FC supported the DAL filter. There were no active electrical or thermal components associated with the DAL-FC. The carrier ring was held in place by a circumferential o-ring at a height that caused the frame of the separate DA filter to be clamped between the carrier and spring devices on the DAL. The DAL filter and carrier were installed together but were not bonded together, allowing any DA filter to be installed with any DA carrier. For the purposes of this enumeration, however, we consider the DAL-FC subassembly, consisting of the separate filter and carrier, to be a fundamental unit of the ApA. The DAL-FC was not integrated in the DA at the time the DA was installed in the dewar but only after the dewar main shell was in place. Until then, a safety plug was installed in its place to protect the CTSL-F.
4. Joule–Thomson baffle (JTB): The JTB was attached to the aperture in the JT shield and provided radiation and contamination baffles.
5. Inner vapor-cooled shield mount (IVCS-M): The IVCS-M was attached to the IVCS and supported the IVCS-FC (#6) via an o-ring. It provided an electrical interface for the heaters and thermometer of the IVCS-FC.
6. Inner vapor-cooled shield filter/carrier (IVCS-FC): The IVCS-FC supported the IVCS filter and associated mechanical, thermal, and electrical components. The IVCS-FC was not installed with the IVCS-M but only after the dewar main shell was in place.
7. Aperture cylinder subassembly (ApC-SA): The ApC-SA consisted of the aperture cylinder tube (ApC-T), bonded to the OVCS mount (OVCS-M) and to the DMS mount (DMS-M). The OVCS-M supported the OVCS-FC (#7) via an o-ring. The ApC-T provided thermal isolation and a vapor barrier. The DMS-M supported the DMS-FC (#8) via an o-ring. The OVCS-M and DMS-M provided electrical interfaces for the heaters and thermometers of the OVCS-FC and DMS-FC. The ApC-SA was attached to the OVCS via thermal straps on the OVCS-M end and was attached to the DMS at the DMS-M end directly, via an o-ring seal. During integration, the connection to the OVCS was made first, and the ApC-SA was supported by its thermal straps until the main shell was installed atop it.
8. Outer vapor-cooled shield filter/carrier (OVCS-FC): The OVCS-FC supported the OVCS filter and associated mechanical, thermal, and electrical components. The OVCS-FC was not installed with the ApC-SA but only after the dewar main shell was in place.
9. Dewar main shell filter/carrier (DMS-FC): The DMS-FC supported the DMS filter and associated mechanical, thermal, and electrical components. The DMS-FC was not installed with the ApC-SA but only after the dewar main shell was in place.

Table 1 Dewar interfaces of the SXS ApA and BFs.

Interface	Standard abbreviation	Nominal temperature
Detector enclosure and heat sink (CTS)	CTS	50 mK
Detector assembly structure	DA	1.3 K
Joule–Thomson cooler interface	JT	4 K
Inner vapor-cooled shield	IVCS	28 K
Outer vapor-cooled shield	OVCS	150 K
Dewar main shell	DMS	250 K

Figure 1(a) is a cross-sectional schematic of the SXS ApA. Note that the CTSL-F, DAL, JTB, IVCS-M, and the ApC-SA were not in physical contact but were held in position by the different temperature stages. Figure 1(b) is the same view without the CTS, with the filter-carrier assemblies removed and shown separately to the side. The four filter carriers (FC) were installed after the dewar main shell was attached.

2.2 *Thermal Design, Analysis, and Performance*

Thermal design drivers for the ApA included minimizing heat transfer between various dewar stages, meeting filter temperature requirements during normal operation, and providing for decontamination of the filters through heaters and interface design. The thermal design was complicated by the steep temperature gradients, the need to establish a seal around each filter to block contamination and radiation, and the accommodations for decontamination heaters on the filters. Key features of the mechanical/structure and thermal design, shown in Fig. 1, were:

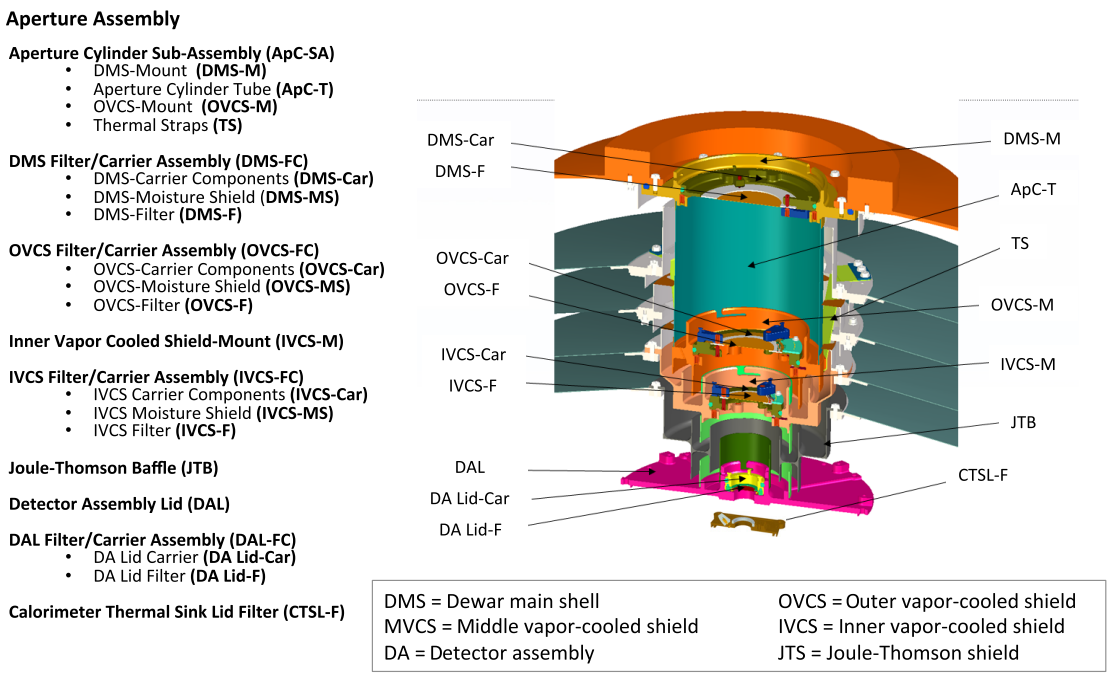

Fig. 1 Schematic cross section showing the arrangement of the Hitomi/SXS ApA and BFs. (a) With FCs installed and position of the fixed CTS filter shown. The thin film of the CTS filter is not shown to instead show the CTS aperture more clearly. (b) With the FCs removed, and the CTS lid not shown. The tops of the dewar shields are also shown, for reference, but the multilayer insulation has been omitted.

1. Thin-walled gamma-alumina/titanium foil tube minimized the thermal conductance between the DMS and the OVCS. The OVCS-M was recessed into the dewar far below the opening in the actual OVCS to maximize the isolation; the length of the tube between its connections to the two mounts was 74 mm.
2. Heat sinking of the OVCS-M to the OVCS was achieved via three thermal straps made of high-conductivity copper.
3. Conductive breaks isolated the OVCS-M, the IVCS-M, JTB, DAL, and CTS.
4. Low emissivity coatings minimized radiation heat transfer. Nested contamination baffles also acted as radiation baffles, minimizing radiative heat transfer between shield-mounted hardware.
5. Filter heaters on the DMS filter allowed continuous heating of the filter to prevent absorption of organic contamination from the spacecraft.

Table 2 Heat flows and temperatures for the SXS ApA.

Interface	In-flight maximum (K)	In-flight minimum (K)	Ground minimum (K)	Benchmark hot case (K)	Predicted heat flow into the dewar shields for benchmark hot case (mW)
DMS	290	233	250	290	N/A
OVCS	179	117	80	152	573
MVCS	130	81	17	111	39
IVCS	49	17	10	28	29
JT	14	4	1.8	4	0.032
DA	1.3	1.3	1.3	1.3	0.009

6. Filter heaters on the OVCS and IVCS filters enabled contingency decontamination of the filters to remove water ice.
7. Filter mounts provided low-conduction contacts to minimize heater power and dewar heat transfer during heater operation.

The DMS and shield temperatures were projected to vary considerably during prelaunch testing and throughout the mission. The minimum shield temperatures occurred on the ground during liquid helium transfers; thus, subsystem testing included these minima, with margin, as survival temperatures. The full range of flight and ground-operation temperatures for the integrated SXS shown in Table 2, including margin (10 K on DMS and 10% on cryogenic components), was used to verify the thermal design by analysis and to establish test ranges. Note that the ground minimum for the DMS filter shown in Table 2 is the actual minimum temperature of the DMS filter recorded during thermal vacuum testing. The nominal hot case temperatures and the resultant heat flows are also shown. This case was important as it was used to determine the He lifetime for the SXS mission. The heat flows shown represent the results from a thermal model (developed using the C&R Technologies, Inc. analysis packages SINDA/FLUINT and C&R Thermal Desktop®). This model was integrated into the dewar thermal model maintained by JAXA and Sumitomo Heavy Industries, the dewar developer. Radiative heat transfer and reflected energy along the exterior of the aperture cylinder were included in the ApA thermal model.

Various thermal properties measured during subsystem thermal-balance testing are summarized in Table 3. The ApC-SA, DMS-FC, and OVCS-FC were tested together in a nonflight apparatus designed to simulate the flight-dewar thermal interfaces and radiation environment. The IVCS-M and IVCS-FC were qualified down to 4 K (using the engineering model parts) and characterized for flight from a liquid nitrogen interface.

Table 3 Significant results of subsystem thermal balance testing.

Property	Value
Thermal conductance of OVCS thermal straps at 150 K (not including contact resistances)	0.55 ± 0.05 W/K (consistent with prediction)
Heat load on 150 K OVCS from 290 K DMS	0.55 ± 0.05 W
Heat load on 150 K OVCS from 240 K DMS	0.37 ± 0.02 W
Typical power to control DMS filter at 320 K when DMS at 290 K and OVCS at 150 K	0.38 W
Typical power to control DMS filter at 320 K when DMS at 240 K and OVCS at 150 K	0.68 W
Typical power to heat OVCS filter to 170 K when OVCS at 150 K and DMS at 290 K	~0 W (filter is radiatively heated by DMS)
Typical power to heat IVCS filter to 170 K from 90 K	0.3 W

2.3 *Resonant Frequencies*

The structural resonant frequencies of the ApA were assessed for each of the major components. A detailed finite element model and closed-form equations were used to identify minimum eigenvalue frequencies. Table 4 summarizes the minimum values, showing the analytical prediction and corresponding requirement. All predicted frequencies are axial (spacecraft Z axis) except the ApC-SA, which is lateral. All results met project requirements.

Due to the size and fragility of the filter and carrier assemblies, frequency measurements were not performed on these components. Results from cold vibration testing of the IVCS-M and FC assembly showed a minimum frequency of 1360 Hz. This was scaled from the ~80 K measurement temperature to the operational temperature of ~20 K. In ApC-SA vibration tests, the minimum frequency was 831 Hz.

There was adequate margin on all clearances under conservative launch loads. The radiation and contamination baffles were designed to meet functional requirements with nominal lateral and axial clearances of ~5 mm.

Table 4 Fundamental frequencies of the SXS ApA subassemblies.

Component	Predicted frequency (Hz)	Minimum frequency requirement (Hz)
ApC-SA	679	150
IVCS-M	1505	150
JTB	613	150
DA lid	388	100
FCs	1424	150
Filters	1333	150

2.4 *Thermomechanical Testing*

A series of tests qualified the basic design features and verified the integrity of the flight units. Thermal and mechanical testing of the three silicon-mesh filters was done in their carriers to provide the appropriate mechanical and thermal interface. Operation of the heaters and thermometers required that the carriers be installed in mounts. These tests are summarized in Table 5. Note that vibration qualification of the ApC-SA with OVCS-FC and DMS-FC was done at room temperature since the nitrogen dewar used for vibration testing would have cooled the cylinder interface to ~80 K, introducing more thermal mismatch at the mount/tube interface than would be present at launch. Vibrating in this condition would be an over test. The under testing of a warm vibration was mitigated by separately measuring the strain at nominal operating temperatures via strain gauges affixed to a prototype cylinder. The measured strain values confirmed the assumptions for thermal strain that had been input to the analysis of the design.

All ApA components that were launched on Hitomi passed their thermomechanical acceptance tests. Spare ApC-SA and IVCS-M units and DA and CTS filters also passed, but some damage was experienced on the IVCS, OVCS, and DMS filters, which resulted in changing their ranking. These minor failures were mostly attributable to factors incidental to the tests themselves, such as from debris, pre-existing defects, or installation tools, as will be discussed along with other lessons learned in Sec. 7.

3 Filter Assemblies

3.1 *Thin-Film Filters and Their Support Structures*

Low temperature x-ray microcalorimeters require very thin filters for rejecting non-x-ray radiation while providing the highest possible transmission in the x-ray band (0.1 to 10 keV). Obtaining high x-ray transmission requires films that are only about 1000 Å thick, composed of polymer film coated with aluminum. These filters have diameters that can be as large as several centimeters (see Table 6) and are extremely delicate. The use of these filters in the ultralow-temperature environment required by the SXS is even more challenging since the filters can become tight when under vacuum (due to moisture loss) and very brittle when cold.

The BFs were designed to prevent radiation with wavelengths longer than x-rays from reaching the detector, where it would heat the pixels or induce photon shot noise. The filters also closed out various thermal shields to minimize heat loads on the cryogens. For the entire stack of filters, the required maximum out-of-band transmission of the filters was 0.006 at 40.8 eV (geo-coronal He II), 0.02 at 21.2 eV, 0.002 at 10.2 eV, and 5×10^{-9} in the IR range (3 to 30 μm). The requirement for attenuation of the geocoronal line was satisfied by the telescope thermal shield, with no additional requirement on the filters. The required minimum in-band transmission for the stack was 16% at 0.6 keV, 52% at 1.0 keV, 70% at 6 keV, and 70% at 10 keV. The attenuation requirements were met by design and measurements from the XRS programs, and the white-light transmission of each filter was measured to assess pinhole transmission. The in-band transmission requirements were verified with x-ray measurements.

The SXS filters used aluminized polyimide and were highly reflective in the visible and IR. The UV attenuation was determined by both the aluminum and polyimide thicknesses. The

Table 5 Thermo-mechanical tests of the SXS ApA. FM, flight model; EM, engineering model.

Test description	Temperature minimum (of test)	Temperature maximum (of test)	Number of cycles or balance points
Warm vibration test of ApC-SA, DMS-FC, and OVCS-FC (EM, FM, spares)	295 K	300 K	N/A
Thermal cycles of aperture tube bonded between OVCS-M and DMS-M	80 K	300 K	Five cycles
ApC-SA thermal gradient/ thermal balance test (EM and FM)	117 K	290 K	Three DMS/ OVCS temperatures
Thermal cycles of DMS-FM and spare carriers	187 K	298 K	Primary and EM: three cycles Spare: six cycles
Heater cycles of DMS-FM and spare carriers	233 K	320 K	10 cycles (11 for EM)
Thermal cycles of OVCS-FM and spare carriers	<100 K	298 K	Primary: three cycles Spare: six cycles
Heater cycles of OVCS-FM and spare carriers	117 K	170 K	10 cycles (11 for EM)
Thermal cycles of IVCS-FM and spare carriers	80 K	290 K	Five cycles
Thermal cycles of IVCS-EM carrier	9 K/85 K	292 K	One cycle to the lower temperature, 1 to 85 K
Heater cycles of IVCS-FM and spare carriers	80 K	170 K	20 cycles
Heater cycles of IVCS-EM carrier	<28 K	170 K	12 cycles
Cold vibration test of IVCS (EM, FM, spares) in mount	80 K	80 K	N/A
Thermal cycles of DA and CTS filters	4 K	295 K	Four cycles (qualification) One cycle (acceptance)
Lifetime test unit (EM spare OVCS-FC) thermal cycles	85 K	290 K	25 cycles
Lifetime test unit (EM spare OVCS-FC) heater cycles	90 K	170 K	12 cycles

Table 6 Locations and aperture diameters of the SXS BFs.

Filter	Nominal distance from the calorimeter array (mm)	Designed diameter (in case of mesh filters, is inscribed circle) (mm)
DMS	192.9	35.0
OVCS	109.9	24.0
IVCS	79.2	18.5
DA lid	26.7	12.0
CTS	5.1	8.6

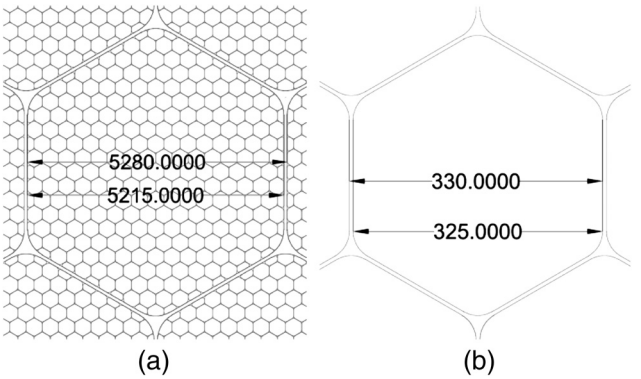

Fig. 2 Dimensions (in microns) of (a) the coarse-mesh and (b) fine-mesh cells of the DMS, OVCS, and IVCS BFs of SXS.

chosen thicknesses came from trading off the high-throughput at low energies, the margin in the thermal design and detector noise budget, and the mechanical strength. Strength is required to survive numerous thermal cycles of low temperatures, mechanical vibration, and pressure gradients of a few hundred Pa. The outer filter was also required to limit the integrated diffusion of helium into the dewar to <0.5 μg, given a required helium pressure in the spacecraft of $<10^{-6}$ Pa. The nominal thicknesses of the films used in the SXS filters are tabulated in Table 7. The composition of each filter was not tailored individually. Instead, two compositions, one for the CTS/DA filters and a thicker one for the IVCS/OVCS/DMS filters, were chosen to meet requirements in aggregate, even in the case of minor damage, such as the development of pinholes. Results of the calibration of the filter transmissions are reported in Ref. 9.

The CTS and DA filters had Al frames and were procured from Luxel Corporation as integrated units. For the DMS, OVCS, and IVCS filters, the silicon-mesh frames were provided by the University of Wisconsin, the aluminized polyethylene terephthalate (PET) close-outs (discussed in Sec. 3.3) were produced at Goddard, and the thin-film filter material was supplied by Luxel. Luxel integrated their thin films with the support frames and close-outs at their facility. Specialized tooling and bake-out procedures were developed by Luxel to optimize contact between the filter film and the silicon grid. The development of the mesh filters was achieved via the collaboration of these three institutions.

The University of Wisconsin developed the monolithic two-level silicon support meshes for the three larger filters. Each mesh contained a coarse hexagonal grid that was 0.2 mm thick. Within each 5.28-mm-wide coarse hexagonal cell was a fine mesh that was either 0.025 mm (IVCS, OVCS) or 0.008 mm (DMS) thick. The layout of the 0.33 mm fine-mesh hexagons was the same in each complete coarse-mesh hexagon, independent of filter type. Figure 2 shows the coarse and fine mesh designs. A backing ring of 0.4-mm-thick Si with the kinematic-mount contact features discussed in Sec. 3.3 was glued to each mesh. Figure 7 is a photo of the OVCS filter that clearly shows the two-level mesh structure. The use of 0.025-mm-thick fine mesh had been initially intended for all three of the mesh-supported filters, but stress fractures that would develop during their fabrication prevented any of the DMS meshes from being completed without damage; thus, the thinner mesh was adopted for these larger filters.

If the pressure limit of the mesh-supported filters were dominated by the burst strength of the polyimide, then mesh filters with the even thinner 45-nm polyimide films of the sounding-rocket payload for which they were originally designed[10] should withstand more than 6000 Pa pressure differences. Such a filter was subjected to a pressure differential of 665 Pa applied in both directions (both pushing the film into and away from the mesh) and survived, but no program was undertaken to test an ensemble of filters to failure. In practice, the increased strength was not used to allow increased pressure differentials (as from increased pumping or venting rates) but only to reduce risk.

The open-area fraction of each two-level structure was over 95%, and the Si became transparent at the top of the SXS bandpass. The meshes were constructed from standard silicon-on-insulator wafers that were produced commercially by bonding two wafers together with an oxide layer and then grinding each side down to the desired thickness. These wafers were procured with the desired thicknesses for the front and backing meshes, and one mesh was patterned and etched from each side with a deep reactive ion plasma etch that produced a vertical profile and stopped on the oxide layer between the wafers. The oxide was then removed from the mesh openings with an acid etch. The silicon structure was completed using epoxy to affix the silicon backing ring containing the kinematic-mount interfaces.

Table 7 Specified thicknesses of the thin films used in the SXS BFs.

Filter or close-out	Aluminum layer	Polymer film
CTS and DA	50 nm	75 nm (polyimide)
IVCS, OVCS, and DMS	100 nm	100 nm (polyimide)
Close-out (MS)	30 nm (×2 sides)	6000 nm (PET)

3.2 *Filter Heaters and Thermometers*

The ApA electrical accommodations included heaters and thermometers on the DMS, OVCS, and IVCS filters. Each of these filters had a thermometer and two separate heater circuits for redundancy. Each heater circuit consisted of several 600-Ω microelectronic resistors in parallel. The thermometer and heaters were bonded to the filter frame via epoxy prior to application of the thin film. Gold wire bonds connected the components to each other and to a printed wiring board. The wire-bonding configuration also provided redundancy for both the heater and thermometer circuits, allowing full functionality even if one bond on the positive side and one bond on the negative were to fail.

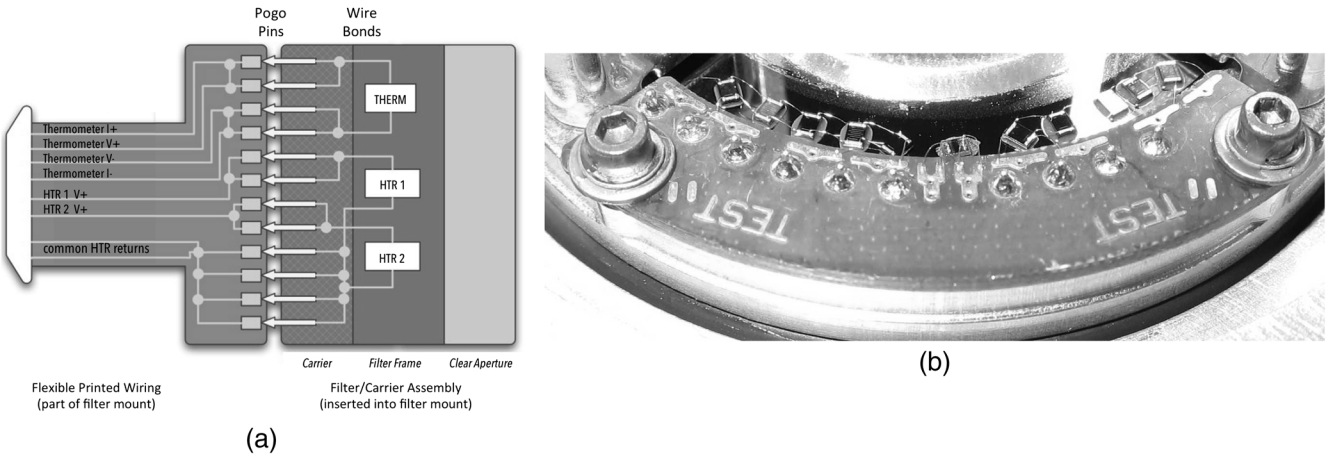

Fig. 3 (a) Electrical schematic of the filter thermometer and heater wiring of a mesh filter and (b) photograph of heater and thermometer components on the IVCS filter.

The DMS resistors also featured double bonds between the series components. Connections between each FC and its mount were provided by spring-loaded pins, which were engaged when the FC was installed into its mount. All connections were made through two spring-loaded pins in parallel, for redundancy. Figure 3 shows the schematic of the redundant circuitry and a photo of the heaters and thermometers on the frame of the IVCS filter.

3.3 *Filter Carriers and Close-Outs*

All filters except the CTS were installed after the dewar main shell was attached. Each of these filters required a carrier to provide the mechanical, thermal, and electrical interface (for IVCS, OVCS, and DMS) between the filter and its mount and the mechanical interface to the installation tool.

The DAL-FC was made from aluminum and coated in gold. The DA BF did not have any electrical or thermal features. The DA filter was simply sandwiched between a set of ball plungers and an o-ring and did not have any rotational alignment requirements. Unlike the other filters, the DA filter and its carrier did not become permanently integrated with each other. Figure 4 shows the CTS and DA filters.

The IVCS, OVCS, and DMS carrier rings were also made from aluminum and coated in gold. Each carrier had a circumferential o-ring that secured it into its respective mount. Additionally, six ball plungers in the mount supported the carrier and adjusted it to its proper height. Each BF was supported in its carrier via a kinematic-mount system that consisted of three ball plungers and three ball-end Ti set screws. Each pair of a ball-end screw and a ball-headed spring plunger supported the filter and engaged with its kinematic-mount features to constrain motion in 3 (triangular notch), 2 (oblong notch), or 1 (flat contact) degrees of freedom. The kinematic mounting allowed for free movement upon differential thermal expansion and contraction. Figure 5 contains a drawing showing the kinematic mount points on the back of the IVCS filter and a photograph of a triangular notch resting on a ball-end screw. The kinematic-mount notches were laser-cut through-holes that were chemically smoothed.

On the IVCS and OVCS-FCs, the structures that held the ball plungers in position also had T-shaped features that were grabbed by the installation and extraction tools. For the DMS carrier, which was inserted with the backing-ring side toward the tool, these pick-up features were on the back of the carrier ring. The orientation of the DMS filter was reversed so that the OVCS and DMS filters could both be installed with the lowest

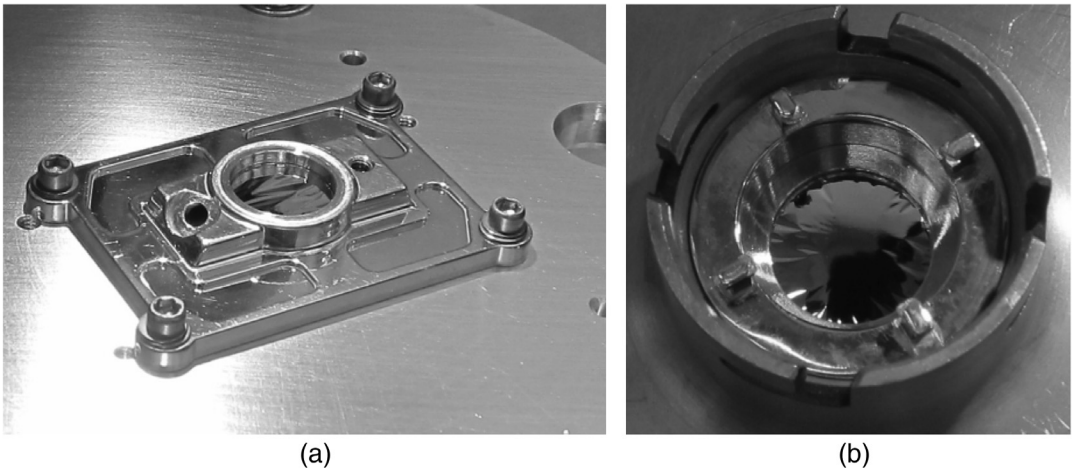

Fig. 4 (a) CTS lid with filter (CTSL-F) and (b) DAL filter and carrier (DAL-FC) in nonflight holder.

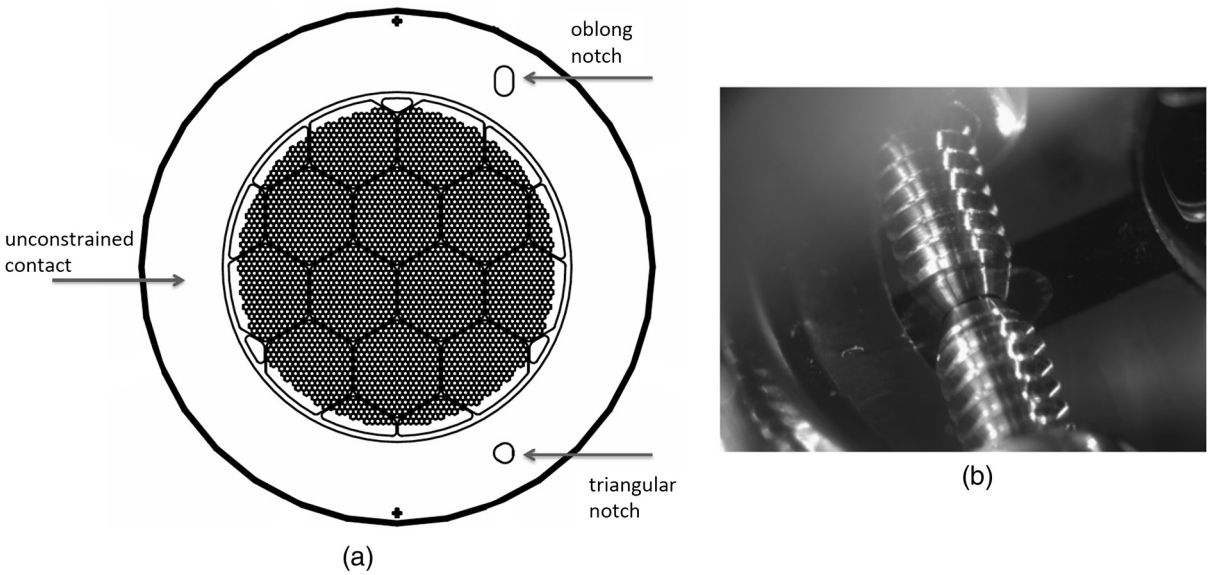

Fig. 5 (a) Kinematic mount points on the back of the IVCS filter. (b) Photograph of a triangular notch resting on a ball-end screw. The reflection of the ball-end screw is seen in the metalized surface of the silicon frame.

emissivity sides facing the inside of the ApC-SA. The DMS ball-plunger structures also had pick-up features but only for easier handling during assembly.

The small gap between the filter frame and the carrier was covered by a moisture shield (MS) that was also referred to as the close-out. The MS was bonded to the filter frame at its inner diameter and to the carrier at its outer diameter, as shown if Figs. 6 and 7. The MS was made of aluminized PET and incorporated a flexible feature to allow for thermal expansion and contraction of the silicon frame with respect to the aluminum carrier ring. This strain-release feature was formed into the

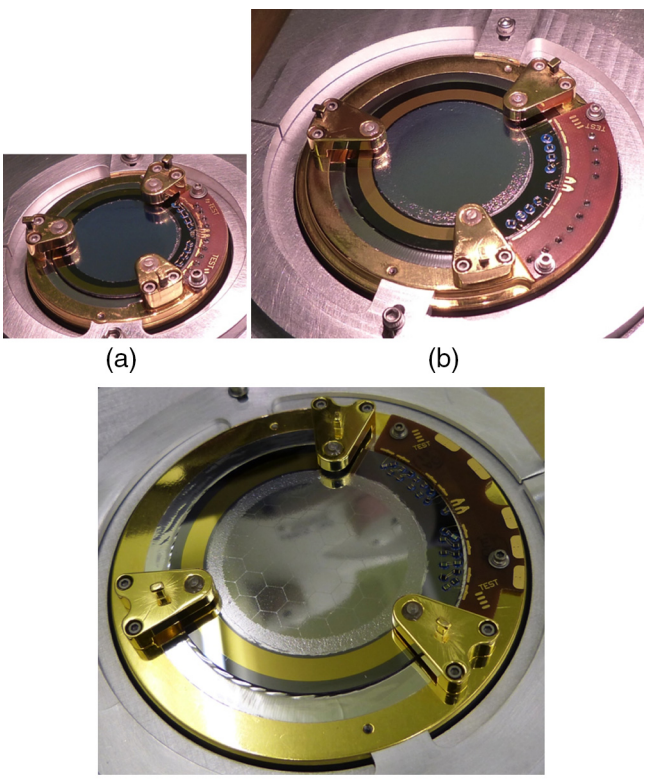

Fig. 6 (a) The IVCS, (b) OVCS, and (c) DMS-FCs for SXS. The three triangular structures in each assembly hold the spring-loaded ball plungers.

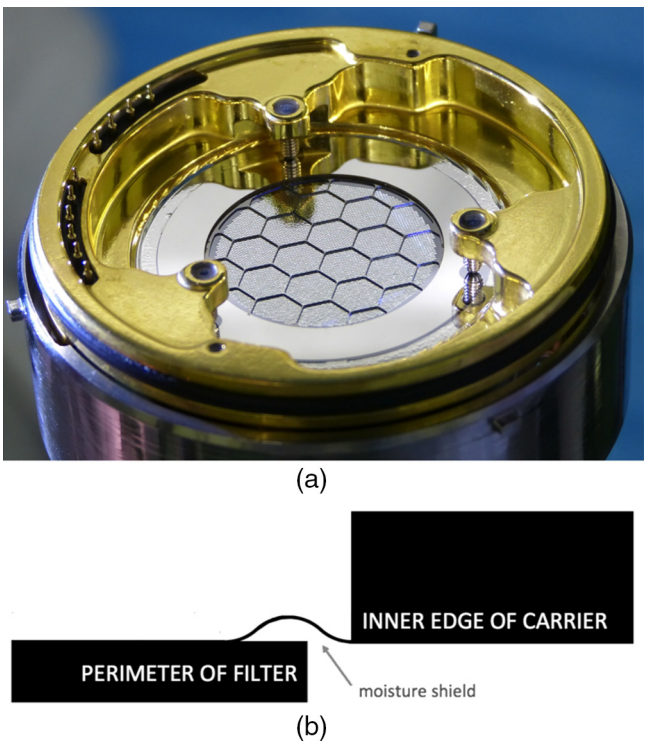

Fig. 7 (a) Photograph of FM OVCS-FC from the back, revealing the coarse and fine silicon-mesh cells, the moisture-shield interface to the silicon frame, the kinematic mounting, and the spring-loaded electrical contacts. (b) Schematic showing how the MS spanned the gap between the filter and carrier ring, attaching to the back of the filter (shown in the photograph) and the top of the carrier (as seen in Fig. 6).

aluminized PET sheet by a heated stainless-steel mold. The MS blocked the passage of light, water vapor, helium, and other contaminants around each filter. Acceptable white-light transmission and helium permeation were verified on samples of the MS material.

The IVCS and OVCS carriers included a printed wiring board (PWB) with spring-loaded contact pins. Wire bonds electrically connected thermometers and heaters to the PWB. The spring pins contacted the electrical contact pads in the mount upon installation. The DMS was similar, but the spring-loaded pins were on the mount side of the interface.

Figure 6 shows the DMS, OVCS, and IVCS-FCs. Figure 7 shows the back of the OVCS-FC while being held in the installation tool. This view clearly shows the two-layer mesh, the backing ring, the kinematic-mounting points, the electrical contacts, and the MS interfaces. The equivalent features of the DMS and IVCS filters were conceptually similar.

3.4 *DMS Filter Heating*

As a result of projected outgassing rates on the spacecraft, various contamination-mitigation schemes were pursued. The solution chosen was to keep the DMS filter temperature continuously controlled at an elevated temperature after the dewar gate valve was opened. The choice of control temperature for the DMS filter depended on an assessment of the most likely contaminants and what the constituents of the filter could safely tolerate. From analysis of spacecraft outgassing, DEHP ($C_{24}H_{38}O_4$) was assumed to be the dominant contaminant, based on the energy-dependent absorption associated with the contamination that accumulated on the Suzaku XIS filters. Measurements of accumulated contamination during baking of the Suzaku spacecraft indicated that the sticking coefficient was zero for surface temperatures >279 K. To allow for uncertainty in the nature of the major contaminant, the dependence on surface properties, and the uncertainty in thermal modeling, the plan established for DMS-filter heating was to maintain all points on the DMS filter at a temperature >300 K.

The filter temperature was limited by the adhesive used in the construction of the filters. Luxel originally advised limiting the filter temperature to <65°C (338 K), but that was a standard limit based on an adhesive that was no longer in use at the time of the construction of the SXS filters. Later, Luxel revised the recommended limit to 100°C (373 K). A test of the spare EM DMS filter showed that the filter could be heated over 420 K without introducing any permanent change to the appearance on microscopic visual inspection. Specifically, there was no damage to the fine mesh, no new tears or pinholes in the thin film, and no apparent migration of the epoxy; however, neither out-of-band nor x-ray transmission measurements were made.

The operating plan was to control the temperature of the DMS filter frame at 320 ± 2 K. The expected required heater power ranged from 0.7 W at the coldest main-shell temperature of 233 K to 0.3 W at a 295 K main-shell temperature, based on subsystem-level testing.

Due to the low thermal conductivity of the silicon mesh and radiative losses from the thin film, the DMS filter was expected to have a gradient from the control thermometer to the center of the mesh in addition to a gradient around the filter frame from the heater/thermometer to 180 deg opposite. SINDA/FLUINT modeling showed that a cold-case DMS temperature of 233 K would result in the highest heater power (850 mW) and therefore the highest gradient, ~23 K. The coolest area was slightly offset from the center. A lower gradient was projected for the hot case due to the reduced heater power (400 mW).

Given that the model predicted a higher power to control the filter temperature than experimentally determined, we sought a secondary method to increase our confidence that the actual temperature gradient across the filter would be acceptable. A simple analytical model was developed to check the SINDA/FLUINT results and fold in actual measurements. This model addressed the radial gradient in the thin film from radiative losses separately from the lateral gradient in the thicker silicon frame of the filter. This model yielded a value for the conductance of the filter to the carrier that was consistent with the heater power needed for both a 295 and 265 K main shell. This conductance in turn showed that the gradient in the filter frame for the cold case would be ~12 K. The gradient within the thin film depended on its emissivity. Using a conservative emissivity of 0.2, the coldest point in the filter would be 16 K lower than its perimeter, assuming a uniform temperature at the boundary. Using a more realistic emissivity, the gradient in the frame would dominate the gradient in the film. This simple model shows that conservative assumptions reproduce the scale of the gradients determined in the SINDA/FLUINT modeling.

There are additional layers of conservatism. The cold case represented an extreme DMS temperature that was lower than the expected minimum. In addition, the plan to keep all points of the DMS filter above 300 K included margin over the minimum temperature of 279 K. Thus, we had confidence that the filter could be maintained at an adequate temperature.

3.5 *OVCS and IVCS Filter Heating*

The OVCS and IVCS filters were cold enough to condense water vapor that was trapped and released slowly by the multilayer-insulation thermal blankets within the cryostat. The DA filter and the CTS filter were also cold enough to condense water vapor, but they were fully enclosed within cold shields and baffles that do not allow the penetration of water vapor. The primary mitigation for water condensation on the OVCS and IVCS filters was the water vapor barrier in the aperture cylinder and baffling. The secondary mitigation was a heater and a corresponding thermometer to monitor the filter frame temperature during operation.

The desorption rate of water is effectively zero below 140 K and increases rapidly above 150 K. The sticking probability of water on a cold surface is unity in this temperature range. According to Speedy et al.,[11] increasing the temperature to 170 K results in a desorption rate of 6 to 12 monolayers per second, depending on the morphology of the ice. Therefore, if ice accumulation was to have become evident in orbit, the IVCS and OVCS filters would be heated to 170 K.

4 Detector-Assembly Lid, Filter Mounts, Aperture Cylinder, and Joule–Thomson Baffle

4.1 *Mounts and Baffles*

As can be seen in Fig. 1, the ApA components from the OVCS to the DA were arranged with interleaving baffles. These baffles were designed to ensure that no molecular contamination would

have a direct line of sight to a filter, but must first encounter a cold baffle surface to which it would stick.

The main bodies of all of the aperture components were made of gold-plated aluminum. Surfaces engaging the installation tool were anodized. The filter receptacles in the DA lid and the IVCS, OVCS, and DMS-M each supported their respective filter via an o-ring groove and six axial ball plungers. Rotational alignment was not required for the DA filter. For the others, a radial slot in the mount provided a visual reference for the rotational alignment, and alignment was actually achieved via the installation tool, which made use of an alignment tab on the carrier. Circumferential tabs on the installation tool engaged slots around each filter receptacle. As the tool pushed the carrier into place, the force was reacted at the tabs.

The IVCS-M and OVCS-M each supported a flat trace harness that terminated on a connector at one end and on a PWB with gold-plated contacts on the other; for the DMS, the PWB contained spring pins. The PWB was located radially and below the o-ring groove in the mount. When the carrier was pressed into position, the spring-loaded pins aligned with the contacts and provided electrical continuity from the filter thermometer and heaters to the connector.

4.2 *Aperture Cylinder*

The aperture cylinder consisted of a two-ply gamma-alumina fiber-epoxy composite with a Ti foil liner that was co-cured into the tube. Gamma-alumina fiber-epoxy was chosen because of its very low thermal conductivity combined with good material strength, which allowed the practical limit of only two diagonal plies to provide adequate mechanical strength. Titanium foil (alloy 15-3-3-3, 0.0127 mm thick) provided a barrier to water. Due to design heritage from XRS, a water permeation test was not performed on either a qualification unit or flight unit of the aperture cylinder. Since water will pass through the Ti only through cracks or pinholes, and not diffusion, a light-leak test was performed as a means of verifying the water permeation requirement. Figure 8 is a photograph of the ApC-SA.

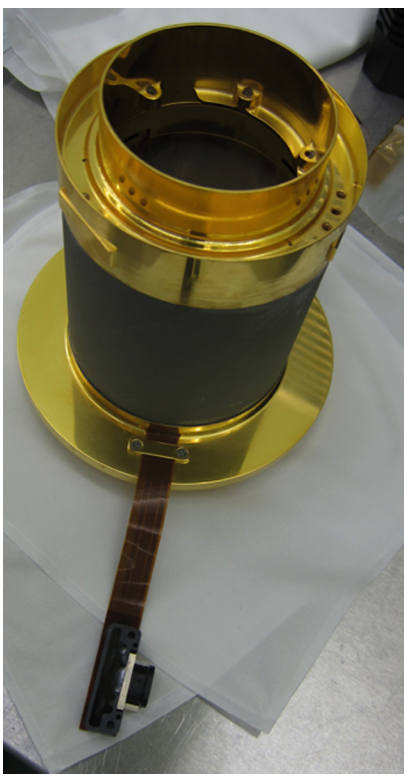

Fig. 8 SXS aperture cylinder subassembly, OVCS side up. The harness seen in this view is for the DMS.

To minimize the pressure differential across the filters to 1 Torr (133 Pa) or less during (i) dewar pump down and (ii) filter installation, a set of venting holes was placed in the OVCS-M. Without these, the ApC-SA would have been a completely enclosed volume. Three 1-mm-diameter holes were positioned 120 deg apart. These had a collective cross-sectional area of 2.36 mm^2 against a total enclosed ApC air volume of 4.73×10^5 mm^3. For a 20-Torr/min dewar pump down, a 1-Torr differential across the filters only required a vent area of 0.005 mm^2, which is equivalent to a factor of 174 area margin. As for filter insertion, a 20-mm/s installation velocity (much faster than the procedure) would require a 0.006-mm^2 vent area, which has an equivalent margin of 135 times.

5 Integration into the Dewar

The separate components of the ApA were integrated into the dewar as the shields and associated multilayer insulation and harnesses of the top (aperture side) of the dewar were built up. The JTB, IVCS-M, and the ApC-SA (OVCS side) each mounted to an adjustable interface ring in its respective shield. The dewar main shell position was pinned. It was the responsibility of JAXA to align the helium tank and shield apertures to the dewar reference. The alignment of the detector and the CTS and DA apertures is discussed in Ref. 8. The JTB, IVCS-M, and the ApC-SA did not use alignment pins. The ApA alignment plan largely relied on having adequate margin in the root-mean-square sum of all the contributions to the clear-aperture budget. The clear aperture at the IVCS had the smallest margin, so a method of locational biasing (use of temporary fasteners of calibrated shank diameter) was readied for usage pending receipt of the alignment report for the IVCS interface ring. Based on the report, it was decided that no bias was needed.

The dewar was inverted for the installation of the FCs to mitigate the risk of particles or objects falling through the filters. The filter installation tools were required to support and clamp each FC during installation. The tool required a capability to be installed primarily by feel, as visibility was limited except for the DMS-M. The outer head of each tool contained tabs that temporarily engaged slots on the FC mounts to provide a reacting force while the inner shaft/head inserted the FC into the mount. This process required a lever with enough mechanical advantage to ensure a quasistatic insertion of the FC until the o-ring seated into its groove in the mount. The o-ring grooves had been sized to retain each FC in place during launch; thus, the required insertion and extraction forces were large, as high as 280 N in mock-ups of DMS-FC installation. This process was required to be completely repeatable and with essentially no mechanism lash shock introduced as the o-ring relaxed as it expanded into its seated location in the mount. Extensive attention to the design and manufacturing tolerance at each interface of the mechanisms, coupled with several design iterations and numerous rehearsal test runs, validated the design and resulted in the flawless installation of the flight FCs. Figure 9 is a photograph of the OVCS-FC being raised into the dewar for installation. The installation tool is shown supported and guided

Fig. 9 Photograph of the OVCS-FC being raised into the SXS dewar for installation. The installation tool is supported and guided by a mechanism attached to the dewar.

by an additional mechanism designed to improve control of the tools during installation.

6 In-Flight Performance

Due to the premature end of the Hitomi mission, very little in-flight performance data were accumulated on the ApA subsystem. The superb early performance of the detectors[12] indicated that the cold filters survived launch. The DMS, OVCS, and IVCS filters passed their electrical and thermal functional tests, reprising the results of ground tests. Continuous DMS temperature control had not yet started at the time of mission loss, but it was controlled for two orbits as part of the checkout. The DMS filter frame was controlled at 320 K while the main shell oscillated between 254 and 259 K. The average power required was 0.48 W, consistent with extrapolation of results from ground testing.

7 Lessons Learned

The thin films of BFs are susceptible to breakage by particles accelerated by test and launch vibration. Throughout the project, management of particles down to the required scale of 50 μm was a continuous preoccupation. Frequent inspections with good lighting and optics were necessary. In several cases, inadequate cleaning at the early stages of component integration resulted in more difficult cleaning operations at a higher level of assembly. In the future, to the extent allowed by the thermal design, pockets that are difficult to inspect and access with cleaning tools are to be avoided.

The DMS, OVCS, and IVCS-FCs were extremely difficult to assemble. Future implementations should strive to make the hand assembly easier and of lower risk to the thin films and fragile silicon meshes. We have identified a large number of improvements that could be made to the design of the silicon meshes, the heaters/thermometer wiring, and the kinematic mounts. The general goal would be to require less precision of the steps that are executed by hand by choice of components and use of guides. For example, in the kinematic-mounting system, we would like to replace the ball plungers with heavy-duty spring pins with a much larger range of travel. The limited travel of the ball plungers required their careful prescreening and precise vertical positioning over each filter.

During the test program, there were several failures ultimately attributed to process and not to design. Tears in an IVCS filter after a vibration test were attributed to loose metal particles found on the carrier. Chipping of the silicon on the edge of a kinematic mount notch after thermal testing was attributed to a pre-existing rough spot on the edge at the point of contact with the ball-end screw, seen in photographs taken before the test. Hairline cracks in the fine mesh in two locations on a DMS filter (and associated tears in the thin film) were attributed to flexing and snapping of the extraction tool used to remove the FC from the ApC-SA after a vibration test. The latter event forced an important redesign of all the FC installation and extraction tools. Note that none of the tears caused a filter to be completely rejected, just lowered in ranking. The DMS tears and cracked mesh noted above were patched using silver epoxy. The IVCS tear was Y-shaped and could not be patched, but loss of a single 0.33-mm cell was acceptable according to the thermal and detector-noise budgets. One of the major benefits of the mesh support was that it made the filters stronger and able to tolerate localized damage.

The EM SXS underwent instrument and spacecraft environmental testing and experienced a similar temperature history to the FM SXS. Months after the launch of Hitomi, the EM SXS was disassembled, providing the opportunity to inspect the EM FCs and ApC-SA. No damage to the ApC-SA was seen. The kinematic-mount contacts of all mesh filters were undamaged, even on the IVCS, for which it was realized after assembly that the contact at the triangular feature had been made in one of the corners of the triangle instead of its center. No damage to the CTS filter or DMS-FC was observed, but there were tears in one OVCS fine-mesh cell and three IVCS fine-mesh cells. Three out of the four damaged cells contained tears that emanated from a point, suggesting particle impact, whereas the fourth, on the IVCS, consisted of two tears emanating from a point on the cell border. During the construction of the FM FCs, both particle management and inspections were greatly improved, and the examination of the EM filters provided a sobering reminder of the importance of those changes. It is not known whether the cause of the damage to the IVCS filter would have also damaged the DA and CTS filters since, in the EM tests, a thick foil was used in place of the thin DA filter to keep potential filter damage from aborting the greater EM test program.

A programmatic consideration for the use of silicon-mesh FCs is that it integrates an extremely fragile component into a complex subassembly that requires an extended test program. As a result, an accident at the subassembly stage has considerable cost. To mitigate this cost for SXS, three FCs of each size were fabricated and fully tested for flight, which was essentially a choice to pay that cost up front. In addition, it should be noted that both programmatic risk and mission risk are mitigated by the robustness of the mesh filters, in comparison with the unsupported filters. Although the mesh filters are subject to more handling than the unsupported filters, they are more tolerant of it than the unsupported films would be. Additionally, the instrument can tolerate rupture of the film in a few fine-mesh cells, but it cannot tolerate loss of an entire filter. Thus, the benefit of integrated decontamination heaters and more fault-tolerant filters was determined to be worth the added programmatic cost of

integrating and testing a large set of silicon-mesh FCs. The same approach will be used on the replacement for SXS on a planned recovery mission.

Disclosures

This paper is based on our contribution to the proceedings of the SPIE Astronomical Telescopes and Instruments meeting held in Edinburgh, United Kingdom, in June 2016.[13]

References

1. C. A. Kilbourne et al., "The design, implementation, and performance of the ASTRO-H SXS calorimeter array and anti-coincidence detector," *Proc. SPIE* **9905**, 99053L (2016).
2. R. L. Kelley et al., "The ASTRO-H high-resolution soft x-ray spectrometer," *Proc. SPIE* **9905**, 99050V (2016).
3. P. J. Shirron et al., "Design and on-orbit operation of the adiabatic demagnetization refrigerator on the ASTRO-H soft x-ray spectrometer instrument," *Proc. SPIE* **9905**, 99053O (2016).
4. R. Fujimoto et al., "Performance of the helium Dewar and cryocoolers of ASTRO-H SXS," *Proc. SPIE* **9905**, 99053S (2016).
5. R. L. Kelley et al., "The Suzaku high resolution x-ray spectrometer," *Publ. Astron. Soc. Jpn.* **59**, S77–S112 (2007).
6. J. L. Tveekrem, R. A. M. Keski-Kuha, and A. T. Webb, "Gas permeability through thin-foil x-ray filters," *Opt. Eng.* **38**, 120–123 (1999).
7. D. A. Grove, "Polyimide x-ray filter substrates optimized for cryogenic temperatures," *Proc. SPIE* **3766**, 386–393 (1999).
8. M. P. Chiao et al., "System design and implementation of the detector assembly of the Astro-H soft x-ray spectrometer," *Proc. SPIE* **9905**, 99053M (2016).
9. M. E. Eckart et al., "Ground calibration of the ASTRO-H soft x-ray spectrometer," *Proc. SPIE* **9905**, 99053W (2016).
10. D. McCammon et al., "The x-ray quantum calorimeter sounding rocket experiment: improvements for the next flight," *J. Low Temp. Phys.* **151**, 715–720 (2008).
11. R. J. Speedy et al., "The evaporation rate, free energy, and entropy of amorphous water at 150 K," *J. Chem. Phys.* **105**, 240–244 (1996).
12. F. S. Porter et al., "In-flight performance of the soft x-ray spectrometer detector system on ASTRO-H," *Proc. SPIE* **9905**, 99050W (2016).
13. C. A. Kilbourne et al., "The design, implementation, and performance of the Astro-H SXS aperture assembly and blocking filters," *Proc. SPIE* **9905**, 99053Q (2016).

Caroline A. Kilbourne has been developing microcalorimeters for high-resolution x-ray spectroscopy since 1987 when, as a Stanford graduate student, she adapted the NASA Goddard calorimeters for use in a hard x-ray inelastic scattering experiment. She came to Goddard as a National Research Council associate in 1992 and joined the staff in 1995. She was an instrument scientist for the Astro-H SXS and will reprise that role for the planned recovery mission.

Biographies for the other authors are not available.